Investigation of mechanical and thermal stresses in HTS bulks with pores during PFM

Santiago Guijosa[1], Kévin Berger[1], Frederic Trillaud[1,2], Melika Hinaje[3]
[1] Université de Lorraine, GREEN, F-54000, Nancy, France
[2] Instituto de Ingeniería, Universidad Nacional Autónoma de México, 04510 CDMX, México
[3] Université de Lorraine, CNRS, LRGP, F-54000, Nancy, France

ABSTRACT – During pulsed-field magnetization (PFM) processes, high-temperature superconducting (HTS) bulks are subjected to significant mechanical stress due to rapid changes in magnetic flux (Lorentz force) and temperature (thermal stress), potentially leading to mechanical failures. This is particularly emphasized by the inherent fabrication-induced defects such as cracks, grain boundaries, and pores. These defects often result in non-uniform trapped magnetic fields that can strongly impact the HTS performance. The present study focuses on the impact of porosity on the trapped magnetic field, temperature, and mechanical stress of REBCO bulks through a 2D transient multiphysics finite element model (FEM).

Keywords – REBCO bulk, porosity, pulsed-field magnetization

1. INTRODUCTION

Magnetized high-temperature superconducting (HTS) bulks can act as pseudo-permanent magnets for electrical and transport applications at low temperatures [1, 2]. Their trapped magnetic flux density can reach several Tesla, often exceeding that of conventional permanent magnets [3], and depends on the average critical current density J_c and bulk size. Manufacturing techniques like top-seeded melt growth (TSMG) and infiltration growth (TSIG) have improved J_c through enhanced flux pinning and homogeneity. However, fabrication defects such as pores, grain boundaries, and cracks remain [4, 5], degrading the homogeneity and intensity of the trapped field [6, 7].

This work focuses on the effect of pores in disk-shaped REBCO bulks during pulsed field magnetization (PFM) [8, 9, 10, 11, 12, 13]. Porosity P is defined as the ratio $100 \times (A_p/A_t)$, where A_p and A_t are the pore and total surface areas, respectively. Pores form during powder compaction or gas diffusion, ranging from 1–10 μm to 50–250 μm [6, 14]. TSMG typically yields 10–30% porosity, whereas TSIG achieves denser structures with about 5% [14].

Porosity reduces mechanical strength [15] and alters magnetic behavior [6]. As ceramic materials, REBCO bulks exhibit high compressive strength (≈100 MPa) but low tensile strength (≈10 MPa), making them vulnerable to fracture during magnetization. In PFM, rapid flux motion and temperature rise induce strong thermal and Lorentz-force stresses [16], potentially initiating cracks. To address these effects, this study incorporates micrometer-scale pores in a 2D finite element model that couples an electromagnetic **H**-formulation with a thermo-mechanical model, implemented in COMSOL Multiphysics® 6.2 [17].

2. MODELING FRAMEWORK

In the proposed 2D model shown in Fig. 1, the HTS bulk domain Ω_{sc} is considered as an infinitely long cylinder encapsulated by an air domain Ω_a. The Ω_{sc} domain includes the presence of pores Ω_p in the shape of small ellipsoids or circles. The external pulsed-field $B_a(t)$ is applied along the axial direction of the infinite cylinder at the air boundary Γ_a. We examine increasing porosity from 0.25% to 2% in steps of 0.25%, with five simulations conducted at each step, for a total of 40 simulations. Since the pore distribution is random, this approach aims to provide a more accurate statistical analysis. In addition, each ellipsoid pore has a random minor axis and major axis in the range of 100-125 μm. All of the chosen parameters and properties used in the simulations (see Table 1) are in agreement with PFM experimental setups and (RE)BCO bulks.

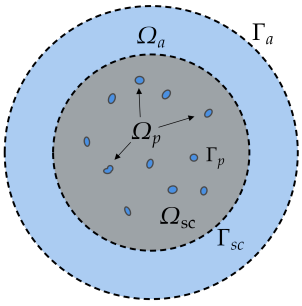

Fig. 1. Schematic drawing not to scale of the different domains and their boundaries: HTS bulk Ω_{sc}, air Ω_a and pores Ω_p (blue ellipsoidal inclusions).

2.1. **H**-*formulation*

The electromagnetic behavior is modeled by solving for the magnetic field **H** according to:

$$\mu_0 \frac{\partial \mathbf{H}}{\partial t} + \nabla \times (\rho \nabla \times \mathbf{H}) = 0 \tag{1}$$

where μ_0 is the permeability of the vacuum and ρ the electrical resistivity of the media. The latter is equal to ρ_a for both Ω_a and Ω_p considering pores as air, and it follows the power law model for the superconducting domain Ω_{sc} given by :

$$\rho_{sc} = \frac{E_c}{J_c} \left(\frac{||\mathbf{J}||}{J_c} \right)^{n-1}. \tag{2}$$

E_c is the critical electric field, n is the index of transition, **J** is the current density and J_c is the critical current density, which depends on the local magnetic flux density and temperature $J_c(\mathbf{B}, T)$.

2.2. *Heat equation*

To evaluate the temperature changes in the superconductor Ω_{sc} caused by the presence of an electrical field **E** and therefore

Table 1. Parameters for the simulation [9, 14, 19].

Parameter	Description	Value
Geometric and electrical properties		
D	Bulk's diameter	29.1 mm
n	Power law exponent	21
E_c	Electric field criteria	1 μV/cm
J_{c0}	Current density constant	500 A/mm^2
J_{c00}	Critical current density at T_0	177 A/mm^2
B_0	Flux density constant	1.3 T
B_m	Max. applied field magnitude	4 T
τ	Pulse time constant	13 ms
Thermal properties		
T_c	Critical temperature	92 K
T_0	Operating temperature	65 K
κ	Thermal conductivity	20 W/(m·K)
α	Thermal expansion coefficient	10^{-5} K^{-1}
c_p	Specific heat capacity	See [9]
Mechanical properties		
v	Poisson's ratio	0.33
Y	Young's modulus	103 GPa
σ_F	Fracture strength	30 MPa
γ_m	Mass density	5900 kg/m^3

of the Joule effect $Q = |\mathbf{E}|\cdot|\mathbf{J}|$, the following equation is solved,

$$\gamma_m c_p \frac{\partial T}{\partial t} - \nabla \cdot (\kappa \nabla T) = Q. \tag{3}$$

Here, γ_m is the mass density, c_p is the specific heat capacity at constant pressure, and κ is the thermal conductivity of the bulk.

2.3. *Mechanical behavior*

Temperature gradients and Lorentz forces ($\mathbf{F}_L = \mathbf{J} \times \mathbf{B}$) emerge during magnetization inducing strains and stresses in the superconductor. The resulting displacement field $\mathbf{u}$ can be solved within the theory of linear elasticity according to,

$$\nabla \cdot \boldsymbol{\sigma} + \mathbf{F}_L = \gamma_m \frac{\partial^2 \mathbf{u}}{\partial t^2}. \tag{4}$$

In these equations, $\boldsymbol{\sigma}$ symbolizes the 2D stress tensor related to the total strain $\boldsymbol{\varepsilon}$ (mechanical and thermal) using Hook's law $\boldsymbol{\sigma} = \mathbf{C}\boldsymbol{\varepsilon}$, where $\mathbf{C}$ is the fourth-order stiffness tensor that contains the material properties. Since ceramics typically experience brittle fracture when one of the normal stress components exceeds the material's tensile or fracture strength σ_F, the primary mechanical parameter used in this work is the maximum stress, defined as $\sigma_{\text{max}} = \max(\sigma_r, \sigma_\theta)$ in a 2D cylindrical coordinate system. This metric, often referred to as the Rankine criterion, is widely used in mechanical analysis, especially for ceramics, as it simplifies complex stress states into a single value that can be directly compared to the fracture strength of the material [18]. Thus, if the maximum stress exceeds the fracture strength, failure occurs.

3. RESULTS AND DISCUSSION

Table 2 compares the ideal (nonporous) case with the average center trapped field, the temperature, and the maximum stress for increasing porosity. The average trapped field decreases linearly with porosity, with a factor of $3.1615P\%$. To simplify the analysis, we focus on porosity percentages of 0.5%, 1%, 1.5%, and 2%, selecting the cases with the lowest trapped field for detailed study. Figure 2 shows that the maximum temperature during magnetization is similar across porosity percentages

Table 2. Statistical analysis for the impact of increasing porosity. Five simulations are averaged and analyzed for each percentage. The average is indicated by the symbol "⟨⟩" followed by the standard deviation marked by "±".

P (%)	$\langle B_z \rangle$ (T)	$\langle$ Max. T $\rangle$ (K)	$\langle \sigma_{max} \rangle$ (MPa)
Ideal	**1.552**	69.7	3.3
0.25	1.543 ± 0.003	77.7 ± 2.5	8.5 ± 2.2
0.5	1.530 ± 0.005	80.0 ± 1.5	8.8 ± 1.2
0.75	1.522 ± 0.004	80.3 ± 2.3	13.2 ± 6.1
1	1.503 ± 0.010	81.0 ± 1.0	11.4 ± 1.5
1.25	1.493 ± 0.004	81.5 ± 1.3	12.8 ± 2.4
1.5	1.477 ± 0.009	81.9 ± 0.5	20.1 ± 5.7
1.75	1.466 ± 0.003	83.1 ± 1.5	21.4 ± 6.4
2	1.451 ± 0.005	82.6 ± 0.9	22.7 ± 6.4

but significantly higher than in the ideal case. Figure 3 shows the maximum stress during PFM, highlighting two tensile stress peaks: one before reaching the maximum applied field and one during pulse descent. The induced tensile stresses approach the average fracture strength of 30 MPa, suggesting that porosity may contribute to crack initiation and propagation, particularly in unreinforced or lower-quality bulks. Notably, the stress during the pulse rise is similar across porosity cases, whereas significant differences appear during pulse descent.

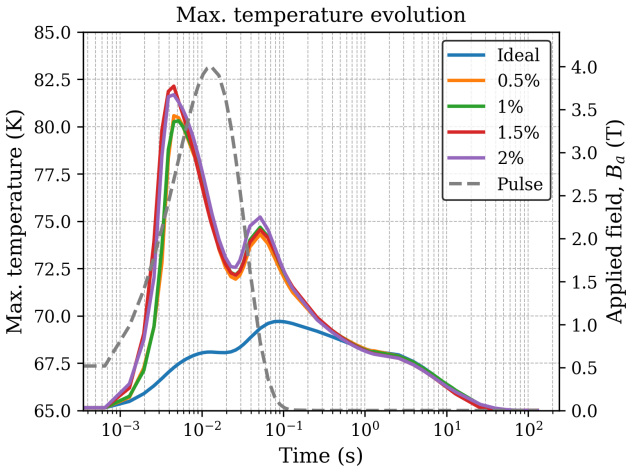

Fig. 2. Maximum temperature evolution during PFM for selected porosity.

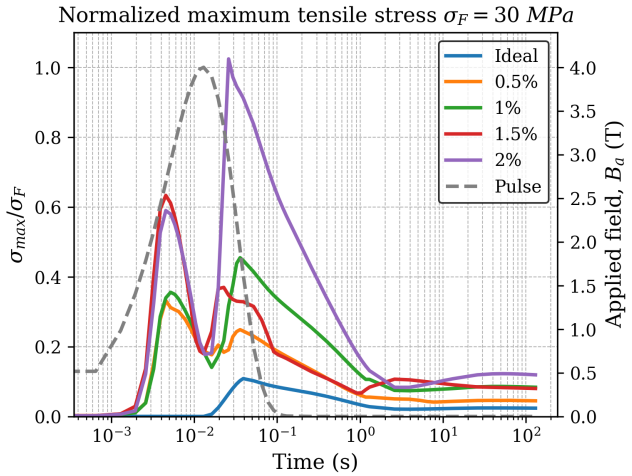

Fig. 3. Maximum normalized ($\sigma_F = 30$ MPa) stress showing different profiles for each porosity percentage, with a clear increase in tensile stress compared to the ideal case.

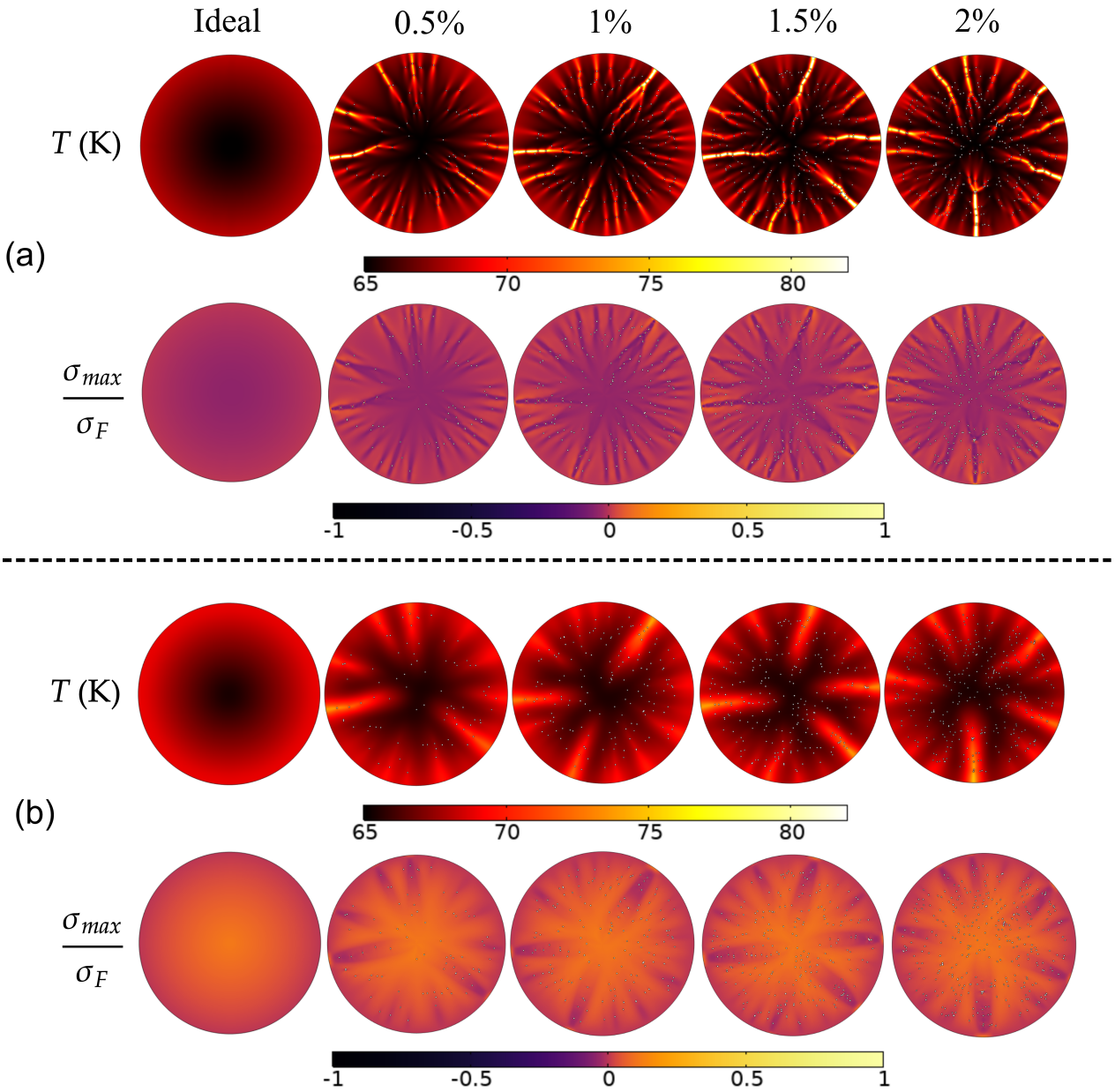

Fig. 4. (a) Comparison of temperature and maximum stress distributions at pulse rise ($t = 4$ ms) for increasing porosity, showing the emergence of lightning-like thermal diffusion patterns, with stress fields closely mirroring these paths. (b) Comparison of temperature and maximum stress distributions at pulse descent ($t = 40$ ms) for increasing porosity. Residual thermal hot spots remain as temperature diffuses, and tensile electromagnetic stresses are concentrated at the bulk center.

Figure 4 (a) shows the comparison of the temperature and maximum normalized stress distribution between the selected porosity cases at pulse ascend ($t = 4$ ms). Temperature lightning-like patterns diffuse towards the center of the bulk and through clusters of pores, followed by the same thermal stresses behavior. This suggests that pores cause a sudden local increase temperature that propagates through the bulk, generating high tensile thermal stresses. Figure 4 (b) presents the same comparison at pulse descend ($t = 4$ ms), showing residual hot spots accompanied by high-tensile stresses at the center of bulk that may be generated from the Lorentz force as the trapped field is relocated towards the center.

4. CONCLUSION

A 2D multiphysics finite element model was developed to investigate the influence of porosity on the thermal, magnetic, and mechanical behavior of REBCO bulks under pulsed field magnetization (PFM). The results indicate that porosity significantly increases local temperature rise, giving rise to lightning-like thermal pathways that propagate through clusters of pores. These localized heat flows generate substantial tensile stresses, potentially threatening the structural integrity of the bulk during the pulse rise phase.

Increased porosity also leads to higher tensile stress levels during the flux trapping stage, particularly at the center of the bulk, highlighting the critical role of pore distribution and relative positioning due to the action of Lorentz forces. Additionally, a linear decrease in the trapped field—quantified as a $3.1615P\%$ reduction at the center—was observed, where P denotes the porosity percentage.

It is worth noting that the current model constrains temperature diffusion to two dimensions, which may result in an overestimation of the temperature rise. A full 3D model would alleviate this limitation and provide a more accurate representation. Future work should include extended modeling and statistical analyses of porosity, incorporating fabrication-induced defects, to better assess their impact on the practical performance limits of HTS bulks.

REFERENCES

[1] J.R. Hull and M. Murakami. Applications of bulk high-temperature superconductors. *Proceedings of the IEEE*, 92(10):1705–1718, 2004.

[2] Q. Wang, H. Zhang, L. Hao, and T. Coombs. Review on high-temperature superconducting trapped field magnets. *Superconductor Science and Technology*, 37(12):123005, nov 2024.

[3] J H Durrell, A R Dennis, J Jaroszynski, M D Ainslie, K G B Palmer, Y-H Shi, A M Campbell, J Hull, M Strasik, E E Hellstrom, and D A Cardwell. A trapped field of 17.6 t in melt-processed, bulk gd-ba-cu-o reinforced with shrink-fit steel. *Superconductor Science and Technology*, 27(8):082001, jun 2014.

[4] G. Krabbes, G. Fuchs, W.R Canders, Hardo M., and R. Palka. *High temperature superconductor bulk materials: fundamentals, processing, properties control, application aspects*. John Wiley & Sons, 2006.

[5] D. K Namburi, Y. Shi, and D. A Cardwell. The processing and properties of bulk (re)bco high temperature superconductors: current status and future perspectives. *Superconductor Science and Technology*, 34(5):053002, mar 2021.

[6] J. Baumann, Y. Shi, D. Weerakonda, J. H. Durrell, and D. A. Cardwell. Understanding the porosity and its effects on the superconducting properties of ybco single grains. *Journal of the European Ceramic Society*, 43(4):1542–1547, 2023.

[7] Q. Nouailhetas, Y. Xing, R. Dorget, W. Dirahoui, S. Guijosa, F. Trillaud, J. Lévêque, J. G Noudem, J. Labbé, and K. Berger. Characterisation of Large-Sized REBaCuO Bulks for Application in Flux Modulation Machines. *Materials*, 17(15):3827, 2024.

[8] K. Berger, J. Leveque, D. Netter, B. Douine, and A. Rezzoug. Influence of temperature and/or field dependences of the $e - j$ power law on trapped magnetic field in bulk ybacuo. *IEEE Transactions on Applied Superconductivity*, 17(2):3028–3031, 2007.

[9] M D Ainslie, H Fujishiro, H Mochizuki, K Takahashi, Y-H Shi, D K Namburi, J Zou, D Zhou, A R Dennis, and D A Cardwell. Enhanced trapped field performance of bulk high-temperature superconductors using split coil, pulsed field magnetization with an iron yoke. *Superconductor Science and Technology*, 29(7):074003, may 2016.

[10] K. Takahashi, M.D. Ainslie, H. Fujishiro, T. Naito, Y-H. Shi, and D.A. Cardwell. Trapped field properties of a y–ba–cu–o bulk by pulsed field magnetization using a split coil inserted by iron yokes with various geometries and electromagnetic properties. *Physica C: Superconductivity and its Applications*, 536:1–10, 2017.

[11] M. D. Ainslie, J. Srpcic, D. Zhou, H. Fujishiro, K. Takahashi, D. A. Cardwell, and J. H. Durrell. Toward optimization of multi-pulse, pulsed field magnetization of bulk high-temperature superconductors. *IEEE Transactions on Applied Superconductivity*, 28(4):1–7, 2018.

[12] H. Fujishiro and T. Naito. Simulation of temperature and magnetic field distribution in superconducting bulk during pulsed field magnetization. *Superconductor Science and Technology*, 23(10):105021, sep 2010.

[13] Kazuya Yokoyama and Tetsuo Oka. Investigation of the magnetizing performance of a rebco bulk magnet excited by pulsed field magnetization using cross-shaped iron yokes. *IEEE Transactions on Applied Superconductivity*, 31(5):1–5, 2021.

[14] D. K Namburi, K Takahashi, T Hirano, T Kamada, H Fujishiro, Y-H Shi, D A Cardwell, J H Durrell, and M D Ainslie. Pulsed-field magnetisation of y-ba-cu-o bulk superconductors fabricated by the infiltration growth technique. *Superconductor Science and Technology*, 33(11):115012, sep 2020.

[15] N Sakai, S.J Seo, K Inoue, T Miyamoto, and M Murakami. Mechanical properties of re–ba–cu–o bulk superconductors. *Physica C: Superconductivity*, 335(1):107–111, 2000.

[16] X. Yang, X. Li, Y. He, X. Wang, and B. Xu. Investigation on stresses of superconductors under pulsed magnetic fields based on multiphysics model. *Physica C: Superconductivity and its Applications*, 535:1–8, 2017.

[17] COMSOL Inc. Comsol multiphysics®, 2024. Accessed: 2024-12-04.

[18] J.A. Collins. *Failure of Materials in Mechanical Design: Analysis, Prediction, Prevention*. Wiley-Interscience publication. Wiley, 1993.

[19] H. Wu, H. Yong, and Y. Zhou. Analysis of mechanical behavior in inhomogeneous high-temperature superconductors under pulsed field magnetization. *Superconductor Science and Technology*, 33(12):124002, oct 2020.